https://doi.org/10.5194/acp-2020-1290
Preprint. Discussion started: 15 January 2021

Atmospheric Chemistry and Physics Discussions

Radiative properties of coated black carbon aggregates: numerical simulations and radiative forcing estimates

Baseerat Romshoo[1], Thomas Müller[1], Sascha Pfeifer[1], Jorge Saturno[2], Andreas Nowak[2], Krzysztof Ciupek[3], Paul Quincey[3], and Alfred Wiedensohler[1]

[1]Leibniz Institute for Tropospheric Research, 04318, Leipzig, Germany
[2]PTB Physikalisch-Technische Bundesanstalt, 38116, Braunschweig, Germany
[3]Environment Department, National Physical Laboratory (NPL), Teddington, TW11 0LW, UK

Correspondence to: Baseerat Romshoo (baseerat@tropos.de)

Abstract. The formation of black carbon fractal aggregates (BCFAs) from combustion and subsequent aging involves several stages resulting in modifications of particle size, morphology, and composition over time. To understand and quantify how each of these modifications influences the BC radiative forcing, the radiative properties of BCFAs are modelled. Owing to the high computational time involved in numerical modelling, there are some gaps in terms of data coverage and knowledge regarding how radiative properties of coated BCFAs vary over the range of different factors (size, shape, and composition). This investigation bridged those gaps by following a state-of-the-art description scheme of BCFAs based on morphology, composition, and wavelength. The BCFAs radiative properties were investigated as a function of the radius of the primary particle (a_o), fractal dimension (D_f), fraction of organics ($f_{organics}$), wavelength (λ), and mobility diameter (D_{mob}). The radiative properties are calculated using the multiple sphere T-matrix (MSTM) method. Amongst size, morphology, and composition, all the radiative properties showed the highest variability with changing size. The cross-sections varied from 0.0001 µm^2 to 0.1 µm^2 for BCFA D_{mob} ranging from 24 nm to 810 nm. After size or D_{mob}, the absorption cross-section (C_{abs}) and BC mass absorption cross-section (MAC_{BC}) showed the highest sensitivity towards composition or $f_{organics}$, whereas the asymmetry parameter (g) showed higher dependence on morphology, which is represented by D_f. The Ångstrom absorption exponent varied from 1.06 up to 3.6 and increases with the fraction of organics ($f_{organics}$). The values of the absorption enhancement factor (E_λ) were found between 1.01 and 3.28 in the visible spectrum. The E_λ was derived from Mie calculations for coated volume equivalent spheres, and from MSTM for coated BCFAs. Mie calculated enhancement factors were found to be larger by a factor of 1.1 to 1.5 than their corresponding values calculated from the MSTM method. It is shown that radiative forcings are highly sensitive towards modifications in morphology and composition. The black carbon radiative forcing ΔF_{TOA} (Wm^{-2}) decreases up to 61% as the BCFA becomes more compact in morphology. Whereas, there is a decrease of >50% in ΔF_{TOA} as the organic content of the particle increase up to 90%. Based on our results, which showed a significant effect of coating and morphology on the BC radiative properties, a parametrization scheme for radiative properties of BC fractal aggregates was developed, which is applicable for modelling, ambient and laboratory-based BC studies. The parameterization scheme for the cross-sections (extinction, absorption, and scattering), single scattering albedo (*SSA*), and asymmetry parameter (g) of pure and coated BCFAs as a function of D_{mob} were derived from tabulated results of the MSTM method. Spanning over an extensive parameter space, the developed parametrization scheme showed promisingly high accuracy up to 98% for the cross-sections, 97% for single scattering albedos (*SSA*), and 82% for asymmetry parameter (g).

1. Introduction

Black carbon (BC), also called light-absorbing carbon (LAC), is produced from incomplete combustion of fossil fuels, biomass, and biofuels, and is reported to be the second largest contributor to global warming after CO_2 with the global forcing estimates ranging between 0.4 to 1.2 W/m^2 (Ramanathan and Carmichael, 2008). It has been found that the annual anthropogenic BC emissions have increased from 6.6 to 7.2 tera-grams during 2000-2010 (Klimont et al., 2017). Moreover, due to rapid urbanization in many developing regions like China, South Asia, South East Asia, the total aerosol mas constitutes of a significantly large portion of BC (Kumar et al., 2018; Bond et al., 2007; Wiedensohler et al., 2002; Madueno et al., 2019, 2020). In addition to the warming effect, BC also decreases snow albedo (Doherty et al, 2010), causes adverse health effects (Janssen et al., 2011), and lowers visibility (Wang et al., 2020).

Radiative properties of BC are of scientific interest because they allow conclusions to be drawn on the nature of the particles and to investigate their radiative impacts (Liu et al., 2015; Safai et al., 2015). After its emission into the atmosphere, BC particles undergo various changes in shape, size, and composition (Fierce et al., 2013). Depending upon the atmospheric conditions after emission, irregularly shaped primary spherules provide active

https://doi.org/10.5194/acp-2020-1290
Preprint. Discussion started: 15 January 2021

Atmospheric Chemistry and Physics Discussions

sites for the deposition of water vapour which causes changes in the hygroscopicity of the particles (Petzold et al., 2005; Peng et al., 2017,). In addition to this, different by-products of burning like organics are deposited around the particles (Siegmann et al., 2002; Rudich et al., 2007). These processes lead to the formation of coatings on BC cores (Bond et al., 2006) and reshaping of the BC particles into more spherical structures (Abel et al., 2003). With the BC particles becoming more compact, an increase in the extinction cross section is observed (Liu et al., 2012). Laboratory and ambient studies also show changes in the radiative properties of BC with an increasing volume of organic coating (Shiraiwa et al., 2010; Cheng et al., 2009). Even though the organic coating is less absorbing in nature, but an increase in the absorption cross section is observed due to the lensing effect (Zhang et al., 2018; Zanatta et al., 2016, Saleh et al., 2015). Numerical modelling has been proven to be helpful in better understanding the effect of the changes that BC particles undergo on their radiative properties (Scarnato et al., 2013; Kahnert, 2010; Smith and Grainger, 2014). The advantage of the modelling studies is the ability and flexibility they offer to simulate BC particles of desired size, shape, and composition, hence improving our understanding of BCFAs at the micro-physical level.

The description of the simulated BC particle plays an essential role in their numerically derived radiative properties. The assumption of BC particles as spheres is widely used by atmospheric scientists, especially in the field of climate modelling (Stier et al., 2004; Ma et al., 2011; Düsing et al.,2018;). In the case of aged BC, it is commonly considered that a spherical BC core is encapsulated inside another sphere representing the coating. This morphology is used in the core-shell Mie theory (Bohren and Huffman, 1983) for obtaining the radiative properties of such particles. Even though this method is simpler, it might result in larger discrepancies when compared to the actual measurements (Wu et al., 2018). Mie theory also overestimates absorption in the visible range of light (Adachi et al., 2010). Electron microscopy results of the samples from laboratory and ambient measurements of BC (Ouf et al., 2016; Dong et al., 2018) showed that the BC particles consist of agglomerates made up of numerous primary particles. It has been observed that these particles show self-similarity when viewed over a range of scales, which is an important characteristic of fractals (Forrest and Witten, 1979). This makes BC particles suitable to be termed as black carbon fractal aggregates (BCFAs), and is used as such throughout this study.

The radiative properties of pure BCFAs, i.e. without any external coating, were investigated by Smith and Grainger (2014), further developing a parametrization for radiative properties of pure BCFAs with respect to the number of primary particles (N_s). With regards to the various ambient and laboratory studies emphasizing the role of organics in influencing the BC absorption and scattering properties, a parametrization scheme for radiative properties of organic coated BCFAs is needed (Zhang et al., 2008, Ouf et al., 2016; Dong et al., 2018, Shiraiwa et al., 2010)

The objective of this investigation is to understand and quantify the changes that BCFAs and their radiative properties undergo by simulating various cases of the BCFAs under an elaborated systematic approach that is designed to span a wide parameter space. The BCFAs cases are classified according to various morphologies, compositions, and wavelengths. This approach of categorization of pure and coated BCFAs is aimed to bridge the gaps that are present in modelled radiative data from the previous studies. The radiative properties were calculated using the T-matrix code (Mackowski et al., 2013) and the findings are presented and discussed with respect to the equivalent mobility diameter (D_{mob}) making it more relevant and comparable for laboratory, and ambient studies in which mobility spectrometers are often used for size classification.

In this study, it is highlighted how modifications in the morphology and composition of BCFAs can further influence the BC radiative forcing. Finally, a parameterization scheme for radiative properties (extinction, scattering, and absorption) of coated BCFAs is developed as a function of size at various morphologies, compositions, and wavelengths.

2. Methods

2.1 Morphology of BCFAs

The formation of BCFAs from combustion is a process involving several stages. Along with BC, a complex mixture of gas-phase organic compounds with a spectrum of molecular structures are co-emitted during incomplete combustion (Siegmann et al., 2002; Gentner et al., 2017). Depending upon the source of burning, different types of polycyclic aromatic hydrocarbons (PAHs) are considered to be the direct pre-cursors of BCFAs (Bockhorn 2009). Small PAHs such as acetylene (C_2H_2) are attached to larger precursor PAHs resulting in the growth of these elementary structures. It is postulated that the nucleation of two large PAHs leads to the formation of small three-dimensional particles with diameters ranging from 1-2 nm (Calcote, 1981).

Processes like surface growth and coagulation of gaseous phase molecules or PAHs leads to the further growth of these particles. The high-resolution transmission electron microscopy (TEM) images revealed these particles to be spherules up to the diameter of 10-30nm specific to the flame (Homann, 1967). These primary particles show a randomly ordered microstructure of graphite layers (Hess et al., 1969). Following the processes of

https://doi.org/10.5194/acp-2020-1290
Preprint. Discussion started: 15 January 2021

Atmospheric Chemistry and Physics Discussions

nucleation and coagulation, the primary particles form larger BCFAs, which subsequently grow by aggregation (Sorensen, 2001). Following this concept of fractal morphology, a mathematical description of fractal aggregates was formulated (Mishchenko et al., 2002):

$$N_s = k_f \left(\frac{R_g}{a_0}\right)^{D_f}, \quad (1)$$

where, a_o is the radius of primary particles, N_s is the number of primary particles, D_f is the fractal dimension, and k_f is a fractal pre-factor. R_g is the radius of gyration, which characterizes the spatial size of the aggregate. It is defined as root means square (rms) distance of the aggregate from its geometrical center as follows:

$$R_g^2 = \frac{1}{N_s} \sum_{i=1}^{N_s} (r_i - r_o)^2 \quad , \quad (2)$$

where, r_i is the position vector of the i^{th} primary particle, and r_o is the position vector of the center of mass of an aggregate with radius of gyration R_g.

The size of a BCFA is determined by two parameters, the radius of the primary particle (a_o) and number of primary particles (N_s). Both are sensitive to the emission source. BCFAs originating from the combustion of biomass have a radius of the primary particle varying between 15- 25 nm (Chakrabarty et al., 2006). On the other hand, emissions from aircraft turbines comprise of primary particles with a radius of 5 nm (Liati et al., 2014). Aggregates emitted from diesel engines have a radius of the primary particle varying between 10 nm and 12 nm (Guarieiro et al., 2018). Some experimental studies indicate that in the atmosphere, the radius of the primary particle is polydisperse in nature varying from 10-100nm (Bescond et al. 2014). Following these studies, Liu et al., 2015 reported differences in the radiative properties of BCFAs due to the monodisperse and polydisperse distribution of the radii of the primary particles. Contrarily, Kahnert (2012b) showed that light absorption measurements are insensitive to the radii of the primary particles, when they fall in the range of 10 – 25nm. For the sake of simplicity, aggregates of monodisperse primary particle size were used in this study.

Further, the reshaping of BCFAs into collapsed, sphere-like structures while ageing can be described by the fractal dimension (D_f) (Sorensen, 2001). The value of D_f increases as an aggregate reshapes into a more spherical particle. A D_f of 3 being the value for a sphere, whereas D_f of 1 represents an open-chain like aggregate. In the early stages of their formation, BCFAs have a fractal dimension (D_f) between 1.5 and 1.9 (China et al., 2014; Wentzel et al., 2003). However, as a consequence of the atmospheric aging, the aggregates transform from being bare to partly coated, embedded in coatings. In this case, the fractal dimension can go up to 2.2 (Wang et al., 2017). The exposure to humidity and foreign coatings can collapse the BCFA into a structure having even a larger fractal dimension up to 2.6. (Zhang et al., 2008; Bambha et al., 2013). Hence, studying BC particles under the assumption of aggregate morphology provides a wider range of parameter space (particle size, primary particle size, and morphology). This is limited to only particle size in case of spherical assumptions.

Aggregates are formed from the random motion of a cluster meeting cluster (Sorensen 2001). If the probability of sticking is considered 1, the process of formation is called the diffusion-limited cluster aggregation (Witten and Sander, 1983). Following this principle, Diffusion-limited algorithms (DLAs) have been developed, which include cluster-cluster aggregation (CCA) (Thouy and Julien, 1994) and particle-cluster aggregation (PCA) methods (Hentschel,1984). In this study, the tunable diffusion limited aggregation (DLA) software developed by Woźniak (2012) was used, which iteratively adds the primary particle one by one, preserving the fractal parameters at each step.

2.2 Description scheme of the simulated BCFAs

The previous modelling studies (Kahnert, 2010; Smith and Grainger, 2014) investigated the radiative properties of pure BCFAs i.e. without any coating. From the simulated radiative properties, parametrization for pure BCFAs with respect to the number of primary particles at various fractal dimensions and wavelengths were given (Smith and Grainger, 2014). Ouf et al. (2016) conducted NEXAFS analysis on BC produced from a diffusion flame-based mini-CAST burner and found that organics (by-products of the combustion) get attached to the edge of graphite crystallites without changing the inner structure of the core. For radiative modelling studies, this laboratory result can be simulated by assuming a spherical coating around each individual BC primary particle (Luo et al., 2018). In order to simulate BCFAs with various fraction of organics ($f_{organics}$), the inner radius of the primary particle (a_i) is fixed to 15 nm. Whereas the outer radius of the primary particle (a_o) consisting of the organics, is varied from 15.1nm to 30nm with the fraction of organics ($f_{organics}$) changing from 1% to 90% respectively. The relationship between the outer radius of the primary particle (a_o), the inner radius of the primary particle (a_i), and the fraction of organics ($f_{organics}$) is shown below:

https://doi.org/10.5194/acp-2020-1290
Preprint. Discussion started: 15 January 2021

Atmospheric Chemistry and Physics Discussions

$$\frac{4}{3}\pi a_i^3 = (1 - f_{\text{organics}})\,\frac{4}{3}\pi a_o^3 \quad . \tag{3}$$

Luo et al., 2018 kept the overall size of aggregates constant to study the sensitivity of radiative properties at various number of primary particles (N_s) and vice-versa. In our study, the size of the BC aggregates is increased gradually studying the subsequent changes in the radiative properties. The radiative properties of BC aggregates were calculated for various cases, following a well-designed description scheme summarized in Fig. 1. All the radiative properties are calculated at three wavelengths in the visible range i.e., 467nm, 530nm and 660nm. The values are chosen following the availability of refractive index at these specific wavelengths from Kim et al, 2014. For pure BC aggregates, the radiative properties were calculated for $1.5 \le D_f \le 2.8$ in steps of 0.1. In case of the coated BC aggregates, the radiative properties are calculated at the above-mentioned wavelengths for $1.5 \le D_f \le 2.2$ in steps of 0.1, and for $1\% \le f_{\text{organics}} \le 90\%$ in increments of 5%. The approach of assuming a spherical coating around each individual BC primary particle results in an unlikely structure for coated BCFAs with $D_f > 2.2$, hence those cases were omitted in this study. Fig. 2 shows a few of the aggregates from the classification at a fixed D_f and f_{organics}. The large dataset obtained from the classification helped in further developing the comprehensive parametrization scheme.

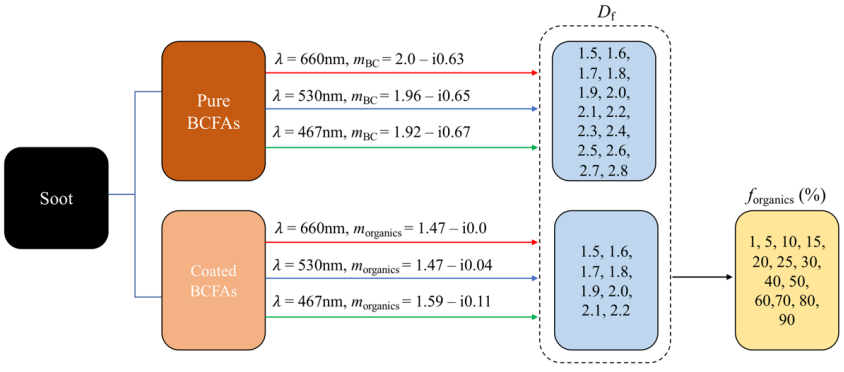

Figure 1. The description scheme of black carbon fractal aggregates (BCFAs) adopted in this study.

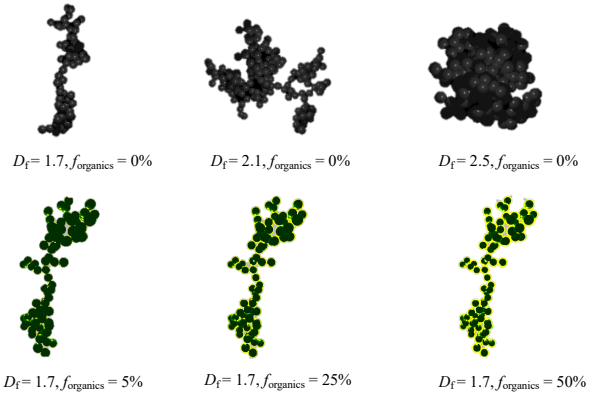

Figure 2. Examples of black carbon fractal aggregates (BCFA) with 200 primary particles, and varying D_f and f_{organics}.

In each case of the mentioned classification, the size of the BCFA is changed by incrementing N_s with 5% and rounded to an integer value, starting from 1 up to 1000. It must be noted that in the results, the size of the BCFA

https://doi.org/10.5194/acp-2020-1290
Preprint. Discussion started: 15 January 2021

Atmospheric Chemistry and Physics Discussions

is expressed in terms of mobility diameter (D_{mob}) instead of the number of primary particles (N_s) using the simple conversion developed by Sorensen (2011) given below:

$$D_{\mathrm{mob}} = 2a_0(10^{-2x+0.92})N_s^x \quad (4)$$

where, x is the mobility mass scaling exponent given by $x = 0.51Kn^{0.043}$, $0.46 < x < 0.56$. Kn is the Knudsen number, which is the ratio of the molecular free path to the agglomerate mobility radius. The estimated error in the mobility mass scaling exponent (x) is ±0.02

The conversion formula given in (4) is well founded over the entire range, spanning from the continuum to free molecular regime. Using the pre-calculated values of x, the mobility diameter (D_{mob}) is derived for the entire dataset. The relationship between derived mobility diameter (D_{mob}), number of primary particles (N_s) and volume equivalent diameter (D_{equ}) for a case of pure BCFA with a_o = 15 nm is shown in Fig. 3.

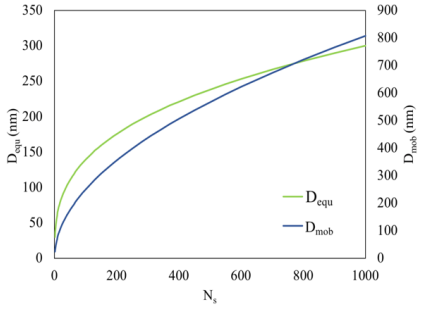

Figure 3. Relationship between mobility diameter (D_{mob}), number of primary particles (N_s) and volume equivalent diameter (D_{equ}) for pure BCFAs with a_o = 15nm.

BC has a refractive index fairly wavelength independent in the visible and near-visible spectrum range (Bond and Bergstrom., 2006). There are modelling studies which assume a wavelength independent refractive index of $m = 1.95 + 0.79i$ for BC over the visible spectrum range (Smith and Grainger., 2014; Luo et al., 2018). For organic carbon, the imaginary part of the refractive index (m_i) is highly wavelength dependent at the shorter wavelengths in the visible and ultraviolent (UV) wavelengths (Moosmüller et al., 2009; Alexander at al., 2008). Contrary to other studies, Kim et al., 2014 concluded that BC shows a fair amount of wavelength dependency, and provided refractive indices for BC and organics in the visible spectrum. Following his study, the real (m_r) and imaginary (m_i) part of the refractive indices used for BC and organics at different wavelengths in this study are summarized in table 1.

Table 1. Refractive indices (m_r and m_i) of BC and organics at various wavelengths in the visible range (Kim et al., 2014) used in this study.

Parameter	Wavelength (*nm*)		
	467	530	660
m_{r_BC}	1.92	1.96	2.0
m_{i_BC}	0.67	0.65	0.63
$m_{r\_Organics}$	1.59	1.47	1.47
$m_{i\_Organics}$	0.11	0.04	0

2.3 Radiative Model – Multi-Sphere T-matrix Method (MSTM)

Multi-sphere T-matrix Method (MSTM) consists of an algorithm for calculating the time-harmonic electromagnetic properties of a set of arbitrary spheres (Mishchenko et al., 2004; Mackowski and Mishchenko, 2011). The MSTM version 3.0 (Mackowski et al., 2013) calculates the radiative properties for fixed and random orientations, the latter being used in this study. MSTM code can calculate the radiative properties of coated BCFAs involving nested spheres with the condition that there should be no intersecting surfaces of individual

https://doi.org/10.5194/acp-2020-1290
Preprint. Discussion started: 15 January 2021

Atmospheric Chemistry and Physics Discussions

primary particles. Radius, and positions vectors of the inner and outer primary particle of the BCFA are obtained from the tunable DLA software (Woźniak, 2012) which is coupled to the MSTM code.
The radiative properties of the aggregates were modelled at three wavelengths, i.e., 467, 530, and 660 nm. At the wavelengths of 660nm and 530nm, the radiative properties from MSTM code are obtained for $1 \leq N_s \leq 1000$. Because of the increasing processing time of the MSTM code at lower wavelengths, the calculations are limited to $1 \leq N_s \leq 500$ at the wavelength of 467nm.

For reference purposes, the radiative properties were also calculated using the Mie theory, and the absorption cross-section from Rayleigh-Debye-Gans (RDG) theory. For the Mie theory calculations, spheres with volume equivalent radius of aggregates were taken. In case of the coated aggregates, a concentric core-shell configuration was used (He at al., 2015). The RGD theory considers the primary particles in the aggregate as individual Rayleigh scatters, while ignoring the inter-particle scattering (Sorensen, 2001). Therefore, in the RGD theory, the total absorption cross-section of the aggregate (C_{abs}^{agg}) is the summation of the absorption cross-sections (C_{abs}^{pp}) of individual primary particles (N_s). For a monodisperse distribution, the absorption cross-section from the RDG theory is given as :

$$C_{abs}^{agg} = N_s C_{abs}^{pp}. \quad (5)$$

2.4 Radiative properties and simplified radiative forcing model

The radiative parameters calculated from the model are briefly presented below. The MSTM code provides the extinction, absorption and scattering efficiency (Q), and the asymmetry parameter (g) of BCFAs. The extinction, absorption and scattering cross–sections ($\mathrm{C_{ext/abs/sca}}$) are further obtained as the product of efficiency (Q) and geometric cross-section ($\mathrm{C_{geo}}$):

$$\mathrm{C_{ext/abs/sca}} = (Q_{\mathrm{ext/abs/sca}}) * \mathrm{C_{geo}} \quad (6)$$

In spherical objects with radii (R), the geometric cross-section ($\mathrm{C_{geo}}$) is simply related to the radius as follows:

$$\mathrm{C_{geo}} = \pi R^2 . \quad (7)$$

Therefore, for a BCFA, the cross-sections ($\mathrm{C_{ext/abs/sca}}$) with volume equivalent radius (R_v) are given as follows:

$$\mathrm{C_{ext/abs/sca}} = Q_{\mathrm{ext/abs/sca}} \pi R_V^2 , \quad (8)$$

The Volume equivalent radius (R_v) is calculated by:

$$\mathrm{R_V} = a_o N_s^{\frac{1}{3}}. \quad (9)$$

The single scattering albedo (ω) is the ratio of scattering efficiency (Q_{sca}) and extinction efficiency (Q_{ext}), where Q_{ext} is the sum of absorption and scattering efficiency as shown below:

$$\omega = \frac{Q_{\mathrm{sca}}}{Q_{\mathrm{ext}}} = \frac{Q_{\mathrm{sca}}}{Q_{\mathrm{sca}} + Q_{\mathrm{abs}}}. \quad (10)$$

Values of ω varies from 0 for a purely absorbing particle to 1 for a completely scattering particle.

Mass absorption cross-section (MAC) is calculated from the ratio of absorption cross section (C_{abs}) and BC mass (m_{BC}) as follows:

$$MAC = \frac{\mathrm{C}_{abs}}{m_{\mathrm{BC}}} = \frac{\mathrm{C}_{abs}}{\frac{4}{3}\pi R_V^3 \rho_{BC}} , \quad (11)$$

where ρ_{BC} is the density of BC fixed to 1.8 g/cm^3 (Bond and Bergstrom, 2006).

The wavelength dependence of light absorption, represented by the Absorption Ångstrom Exponent (AAE) is calculated using the absorption cross-section (C_{abs}) at the three wavelengths (λ) of 467, 530, and 660 nm. The AAE value is obtained as follows:

$$C_{abs}(\lambda = 467, 530, 660) = b\lambda^{-AAE} , \quad (12)$$

where b is a constant.

https://doi.org/10.5194/acp-2020-1290
Preprint. Discussion started: 15 January 2021

Atmospheric Chemistry and Physics Discussions

The amplification in the absorption by ageing of BCFAs can be well quantified from the absorption enhancement factor (E_λ) which is the ratio of absorption cross section of coated BCFA (C_{abs}^{coated}) and pure BCFA(C_{abs}^{pure}) as shown below:

$$E_\lambda = \frac{C_{abs}^{coated}}{C_{abs}^{pure}}. \quad (13)$$

This implies that the enhancement is given for particles of different total mass but the same BC mass.

To understand the atmospheric implication, the radiative forcing is estimated using a model for absorbing aerosols given by Chylek and Wong, 1995. The black carbon radiative forcing at the top of the atmosphere is calculated as:

$$\Delta F_{TOA} = -\frac{S_o}{4}(1 - N_{cloud})T^2 2\tau[(1-a)^2\beta\omega - 2a(1-\omega)] \quad (14)$$

where, $S_o$is the solar constant, $N_{cloud}$is the cloud fraction, T is the transmittance of the sky above the layer of aerosols, τ is the aerosol optical depth, β is the upward scattering function, a is the surface albedo, and ω is the single scattering albedo. From Sagan and Pollack, 1967, the upward scattering function β is calculated from the asymmetry parameter g as:

$$\beta = \frac{1}{2}(1 - g) \quad (15)$$

It is important to note that this is an analytical model which can be useful to understand the sensitivities of radiative forcing to various parameters (Chylek and Wong, 1995; Lesins et al., 2002). However, the model cannot be used to replace the accurate direct radiative forcing calculations.

3 Results and discussion

3.1 Variability in radiative properties due to randomized particle generation

In the tunable DLA program, the user specified values of number of spheres (N_s), radius of the primary particle (a_o), and fractal dimension (D_f) are used to generate the fractal aggregate. This gives rise to a possibility of more than one representation of a fractal aggregate satisfying the same fractal dimension (D_f) i.e. randomized particle generation. The difference between the various representations being only the different positions of the primary particles constituting the aggregate. This further results in an uncertainty in the radiative results. Depending on the complexity, some studies averaged the radiative results over 5-10 representations (Wu et al., 2016; Luo et al., 2018), whereas others consider only a single representation (Smith and Grainger, 2014).

Considering the large dataset in this study, the option of taking an average of the multiple representations would be time-consuming. Therefore, the general uncertainty in radiative properties for 30 representations of the pure BCFAs is discussed. This is done for various cases of size (D_{mob}) and morphology (D_f). Fig. 4 shows the variability in the extinction cross-section C_{ext} (first row), absorption cross-section C_{abs} (second row), scattering cross-section C_{sca} (third row), and asymmetry parameter g (fourth row) as a function of D_f. The results were calculated at a wavelength of 660 nm for pure BCFAs of D_{mob} values 150nm, 250nm, 500nm, and 1000nm increasing from left to right in the Fig. 4.

In order to study the uncertainty in the radiative properties for 30 representations of a BCFA with respect to the modelled fractal dimension, two things must be noted. Firstly, the amount of variability in the radiative property at each fractal dimension (x-axis) must be seen from the height of the boxplot in Fig. 4. Secondly, to see how distinct the radiative properties are with respect to each fractal dimension, the amount of overlapping of the y-axis values between adjacent boxplots must be observed.

For extinction and scattering cross-sections (first and third row), the uncertainty is more pronounced at $D_f <$ 1.7. This is because of the overlapping of extinction and scattering cross-sections values at $D_f < 1.7$. The absorption cross-section (C_{abs}) shows the highest uncertainty towards various representations of a BCFA which can be seen from higher heights of boxplots in panel (e), (f), and (g) of the Fig. 4. Additionally, at 150 nm and 250 nm, C_{abs} values between adjacent boxplots overlap for $1.5 < D_f < 2$. Whereas, for boxplots in panel (g) representing a 500nm BCFA, the C_{abs} values overlap for $D_f > 1.8$. It may be noted that the C_{abs} increases with D_f for smaller BCFA (panel (e) and (f)), whereas the opposite is true for larger BCFA (panel (g) and (h)) as also reported by Luo et al, 2018. This is further explained in detail in the section 3.3. The asymmetry parameter (g) shows a similar uncertainty trend to that of the extinction and scattering cross-sections i.e. lower variability but some overlapping at certain D_f seen in fourth row. In general, it is observed that the uncertainty of radiative

https://doi.org/10.5194/acp-2020-1290
Preprint. Discussion started: 15 January 2021

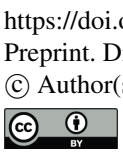

Atmospheric Chemistry and Physics Discussions

properties at larger sizes (D_{mob} =1000nm; last column) is comparatively low. The standard deviation in the radiative properties are averaged over size, and summarized for various cases of D_f in Table 2.

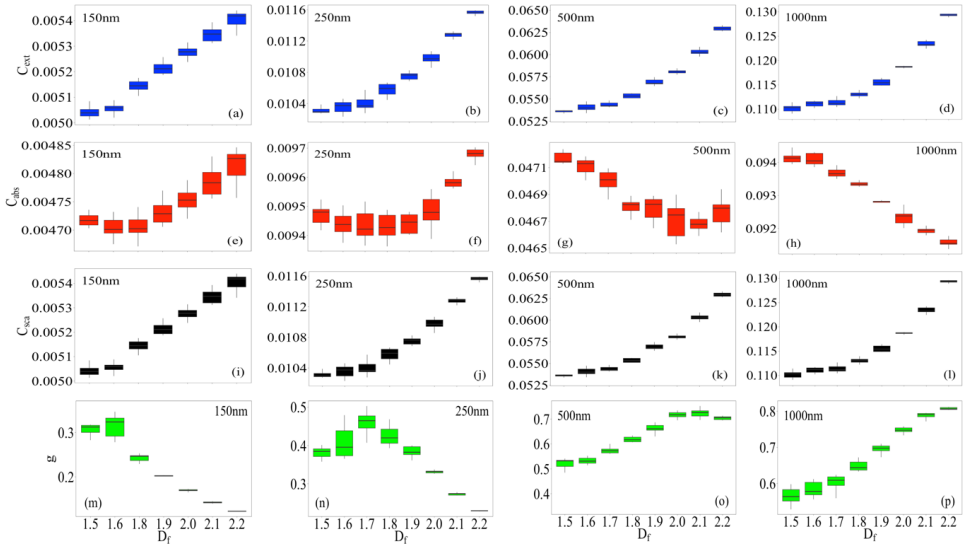

Figure 4. The variability in the radiative properties at $\lambda = 660$nm for 30 representations of pure BCFAs with D_{mob} increasing (left to right). The panels show extinction cross-section C_{ext} (first row), absorption cross-section C_{abs} (second row), scattering cross-section C_{sca} (third row), and asymmetry parameter g (fourth row).

Table 2. Results of variability (%) in extinction cross-section C_{ext}, absorption cross-section C_{abs}, scattering cross-section C_{sca}, asymmetry parameter g, and single scattering albedo SSA. An average over the sizes of 100, 500, and 1000nm were taken. The table shows the standard deviation for various cases of fractal dimension (D_f) from 1.5 up to 2.2.

Radiative property	Fractal dimension (D_f)							
	1.5	1.6	1.7	1.8	1.9	2	2.1	2.2
C_{ext}	0.54	0.75	0.65	0.56	0.54	0.46	0.73	0.73
C_{abs}	0.24	0.26	0.34	0.24	0.20	0.39	0.36	0.36
C_{sca}	4.68	5.90	4.68	3.25	2.68	1.52	2.97	2.97
g	5.81	5.24	4.32	2.90	1.76	1.45	3.36	1.56
SSA	4.20	5.29	4.09	2.71	2.17	1.17	2.29	2.29

3.2 Radiative properties of BCFAs at different radius of the primary particle

The absorption cross-section (C_{abs}) and BC mass absorption cross-section (MAC_{BC}) have been reported to be insensitive to radius of the primary particle (a_o) for a fixed particle volume (Kahnert, 2016b). Fig. 5 shows the radiative properties of pure BCFAs with the radius of primary particle (a_o) varying between 15nm and 30nm as a function of D_{mob}. The results were calculated at a wavelength of 660nm for pure BCFAs with D_f of 1.7. The C_{abs} showed in panel (b) increases by a factor of almost ten from a_o equal to 15nm to 30nm due to the higher electromagnetic field interaction. They are not expected to follow the findings of Kahnert, 2016b, since the results here are represented against the D_{mob} instead of volume equivalent radius (R_{equ}). The results with respect to the R_{equ} are provided in the Fig. S1, which follow the findings of Kahnert, 2016b. The asymmetry parameter shows the least dependency on a_o seen in panel (d). The single scattering albedo (SSA) and the BC mass absorption cross-section (MAC_{BC}) shown in panel (e) and (d) of the Fig. 5 show a larger increase at a_o> 20nm for the same D_{mob}. Acknowledging the effect of changing $a_o$over the radiative properties, for the sake of better relevance and

https://doi.org/10.5194/acp-2020-1290
Preprint. Discussion started: 15 January 2021

Atmospheric Chemistry and Physics Discussions

comparisons, in this study the inner radius of the primary particle (a_i) was fixed to 15nm, and the outer radii of the primary particle (a_o) was increased with $f_{organics}$.

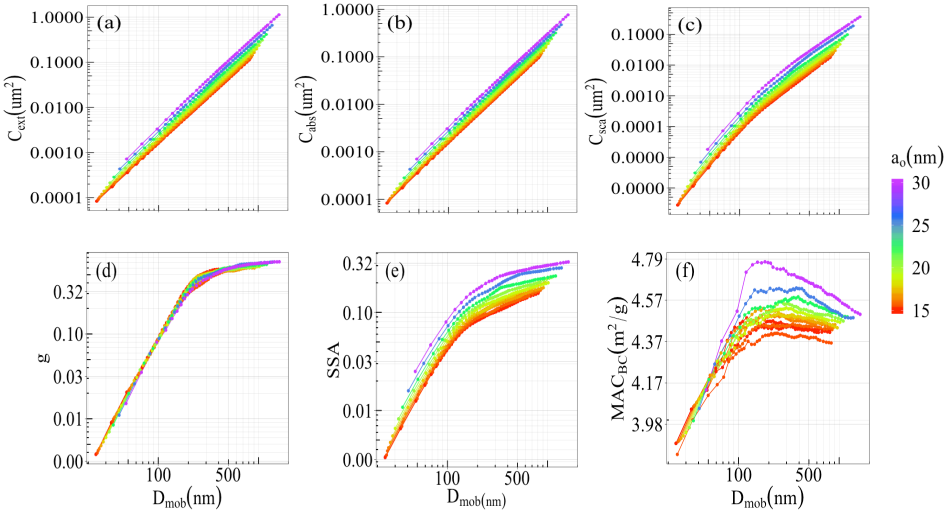

Figure 5. Radiative properties of pure BCFAs at various radius of primary particle (a_o) with respect to mobility diameter (D_{mob}): extinction cross-section C_{ext} (a), absorption cross-section C_{abs} (b), scattering cross-section C_{sca} (c), asymmetry parameter g (d), single scattering albedo SSA (e), and black carbon mass absorption cross-section MAC_{BC} (f) at λ = 660nm.

3.3 Dependency of BCFA radiative properties on the morphology

Different radiative properties as a function of changing size or D_{mob}, and morphology or D_f are shown in Fig. 6. The results were calculated for pure BCFAs ($f_{organics}$ = 0) at a wavelength of 660nm. The cross-sections (panel (a), (b), and (c)) show a coherent increase with D_{mob} with size. The cross-sections vary from 0.0001μm^2 to 0.1μm^2 for BCFA D_{mob} ranging from 24nm to 810nm.The extinction and scattering cross-sections are larger for higher D_f, suggesting an increasing coherent scattering for compact morphologies also reported by Smith and Grainger (2014). The results from Mie calculations for a spherical particle (D_f = 3) follows the trend of the MSTM results as seen in the Fig. 6.

For smaller BCFAs, the absorption cross-section shows negligible dependence on D_f. With increasing size, the absorption cross-section decreases with D_f. This decrease can be interpreted as a shielding effect due to the primary particles on the surface of the aggregate. Further, with D_f > 2.5, the absorption cross-section increases with D_f showing the highest value for a spherical particle (D_f = 3). This may be caused by Mie resonances in larger BCFAs. Earlier studies have also reported higher values for the sphere equivalent (D_f = 3) calculations of BCFA (Liu et al., 2018; Li et al., 2016).

The single scattering albedo (SSA = C_{sca}/C_{ext}) shown in panel (e) of Fig. 6 has values up to 0.42. The SSA also increases with D_{mob} and D_f, the latter is explained by the decreasing scattering in loosely packed BCFAs. This is due to compact aggregates following a Rayleigh-like polarization curve (Gustafson and Kolokolova, 1999). The asymmetry parameter (g) shows a range of values between 0 until 1 over BCFA D_{mob} values of 24nm to 810nm. The g is higher for chain-like BCFAs with lower D_f, indicating larger forward scattering in asymmetrical structures also reported by Luo et al. 2018. When the BCFAs grow larger in size, g gradually decreases for loosely packed ones since the scattering is tending to the Rayleigh scattering regime.

Black carbon mass absorption cross-section (MAC_{BC}) values shown in panel (f) fall within the range of findings reported in the literature (Bond and Bergstrom, 2006). The MAC_{BC} increase with D_{mob} showing a peak at D_{mob} ~ 250nm. The dependency of MAC_{BC} on D_f is similar to that of the absorption cross-section i.e., Mie resonances contribute to the increase at higher D_f, explaining the large discrepancy between MSTM and Mie results for MAC_{BC}. The above results with respect to the R_{equ} are provided in the Fig. S2.

https://doi.org/10.5194/acp-2020-1290
Preprint. Discussion started: 15 January 2021

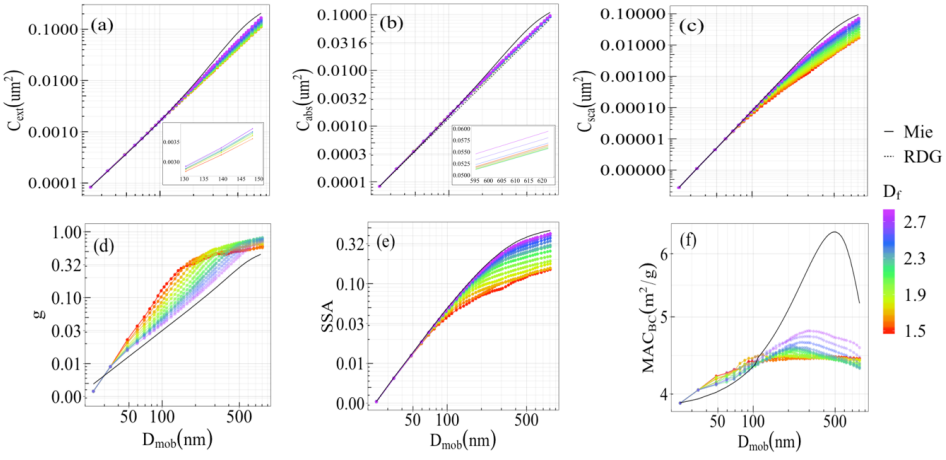

Figure 6. Radiative properties of pure BCFAs as a function of D_{mob} at various fractal dimension (D_f): extinction cross-section C_{ext} (a), absorption cross-section C_{abs} (b), scattering cross-section C_{sca} (c), asymmetry parameter g (d), single scattering albedo SSA (e), and black carbon mass absorption cross-section MAC_{BC} (f) at λ = 660nm. Radiative results from the Mie calculations are shown by the black line (panel a-f). The C_{abs} from the Rayleigh-Debye-Gans (RDG) theory is represented by a dash line (panel b).

3.4 Dependency of BCFA radiative properties on $f_{organics}$

Figure 7 shows how the radiative properties of BCFAs are influenced by the increasing content of organics. The calculations were done for a BCFA of chain-like morphology with D_f =1.7 at a wavelength of 660nm. The results are shown as function of D_{mob} at various fractions of organics ($f_{organics}$). The extinction and absorbing cross-sections (panel (a) and (b)) decrease steadily with $f_{organics}$ because of the increasing less-absorbing volume fraction in the aggregate. The dependence on the asymmetry parameter g (panel (d)) on $f_{organics}$ is very small, meaning that g is more sensitive to morphology rather than composition. The single scattering albedo (SSA) increases with $f_{organics}$, and this is again because of the increasing fraction of less absorbing material. From the results of black carbon mass absorption cross-section (MAC_{BC}) values shown in panel (f), a dominating dependence of BCFA on composition is seen, in comparison to size and morphology. Similar results for a compact BCFA of D_f =2.2 at a wavelength of 660nm can be found in the Fig. S4.

Figure 8 is similar to Fig.6 and shows the dependency of radiative properties on fractal dimension (D_f) for organic coated BCFAs with $f_{organics}$ of 50% at the wavelength of 660nm. The cross-sections and asymmetry parameter show similar behaviour such as that of the pure BCFAs. The SSA has an upper limit of 0.35 at D_f=2.2. Black carbon mass absorption cross-section (MAC_{BC}) values increase by a magnitude of 1.2 for coated BCFAs with $f_{organics}$ of 50%.

Global models use Mie theory for calculations of BC radiative properties (Bond et al., 2013). The Mie theory considers BC as homogeneously mixed spheres, or as a core-shell configuration. The results of SSA, g, and MAC_{BC} in both Fig.6 and Fig.8 clearly demonstrate a significant influence of morphology. This is clearly seen from the difference between the coloured lines representing various morphologies of BC as aggregates, and the black solid line representing the result when BC is assumed as a core-shell. Therefore, the factor of changing morphology is overlooked when using the Mie theory for BC radiative properties in global models.

https://doi.org/10.5194/acp-2020-1290
Preprint. Discussion started: 15 January 2021

Atmospheric Chemistry and Physics Discussions

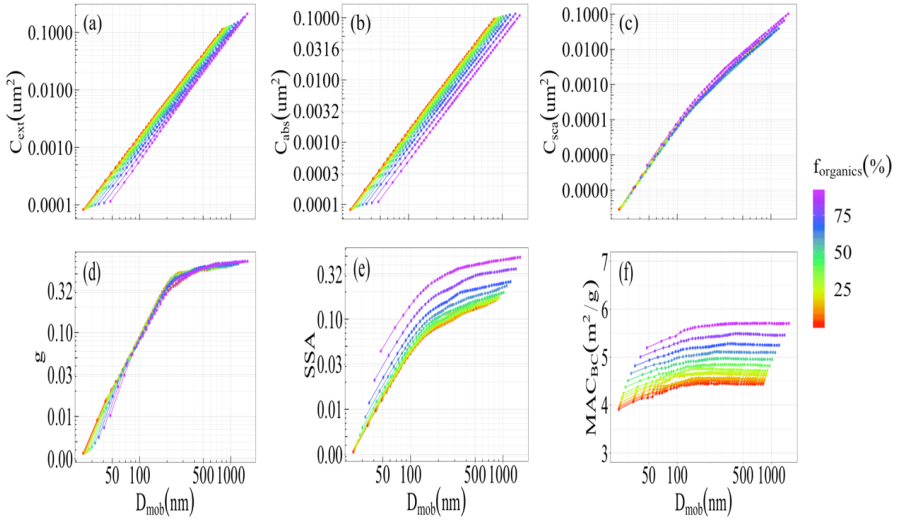

Figure 7. Radiative properties of BCFAs (D_f = 1.7) as a function of D_{mob} at various fraction of organics ($f_{organics}$): extinction cross-section C_{ext} (a), absorption cross-section C_{abs} (b), scattering cross-section C_{sca} (c), asymmetry parameter g (d), single scattering albedo SSA (e), and black carbon mass absorption cross-section MAC_{BC} (f) at λ = 660nm.

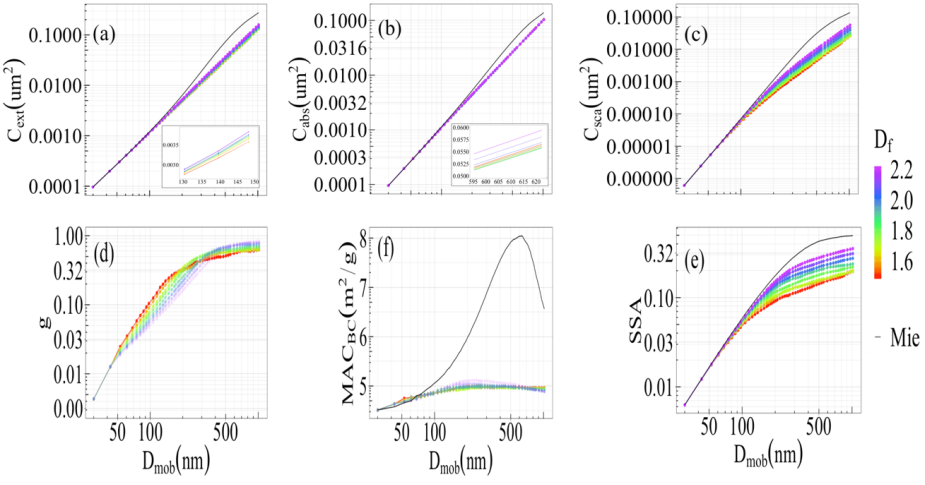

Figure 8. Radiative properties of coated BCFAs ($f_{organics}$ = 50%) as a function of D_{mob} at various fractal dimension (D_f): extinction cross-section C_{ext} (a), absorption cross-section C_{abs} (b), scattering cross-section C_{sca} (c), asymmetry parameter g (d), single scattering albedo SSA (e), and black carbon mass absorption cross-section MAC_{BC} (f) at λ = 660nm.

https://doi.org/10.5194/acp-2020-1290
Preprint. Discussion started: 15 January 2021

Atmospheric Chemistry and Physics Discussions

3.5 Dependency of BCFA radiative properties on wavelength

In the sections before, the dependency of BCFA radiative properties on size, morphology, and composition were discussed. In this section, besides showing the spectral dependency of BCFA radiative properties, it is also demonstrated how this dependency changes with morphology, and composition in the visible wavelength range. Figure 9 shows the changes in the pure BCFAs radiative properties with wavelength (λ) at various morphologies represented by D_f. Pure BCFAs with fixed D_{mob} equal to 330nm were taken for this case to demonstrate the effect of morphology. All the radiative properties show a decrease with λ in the visible range. Further, it was studied whether the rate of decrease might vary for various morphologies. The spectral dependency is insensitive to morphology for the absorption cross-section C_{abs} (panel (b)) and black carbon mass absorption cross-section MAC_{BC} (panel (f)). The spectral dependence of scattering cross-section C_{sca} (panel (c)) is seen to be somewhat sensitive towards changes in morphology. The highest sensitivity of spectral dependence to morphology was seen for the asymmetry parameter (g), dominant at higher D_f i.e. for compact aggregates.

Figure 10 is provided to illustrate how the spectral dependency of BCFAs changes with composition i.e. fraction of organics ($f_{organics}$). For this case, BCFAs are considered with N_s and D_f equal to 200 and 1.7 respectively. It must be noted that the size of the BCFAs are also increasing with $f_{organics}$. Contrary to the results from Fig. 9, all the cross-sections (panel (a), (b), and (c)) and black carbon mass absorption cross-section MAC_{BC} (panel (f)) show a significant increase in the spectral dependency with $f_{organics}$. The spectral dependency of single scattering albedo SSA (panel (d)) shows a comparatively lower sensitivity towards $f_{organics}$, whereas it's nearly negligible for the asymmetry parameter (g) seen in panel (e). Additionally, the change in spectral dependency over the size is also shown in the Fig. S5.

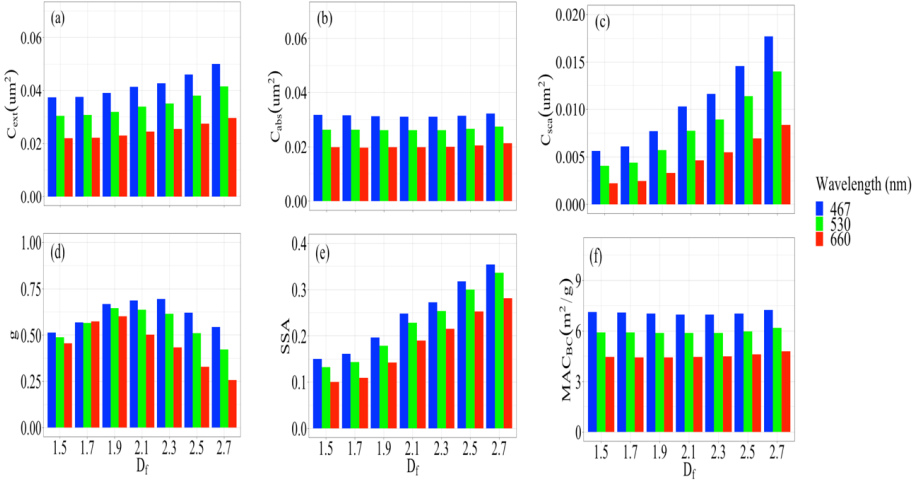

Figure 9. Spectral dependency of the pure BCFAs radiative properties (D_{mob} = 330nm) on fractal dimension (D_f): extinction cross-section C_{ext} (a), absorption cross-section C_{abs} (b), scattering cross-section C_{sca} (c), asymmetry parameter g (d), single scattering albedo SSA (e), and black carbon mass absorption cross-section MAC_{BC} (f). For the variability (%) in different cases of D_f refer to Table 2.

https://doi.org/10.5194/acp-2020-1290
Preprint. Discussion started: 15 January 2021

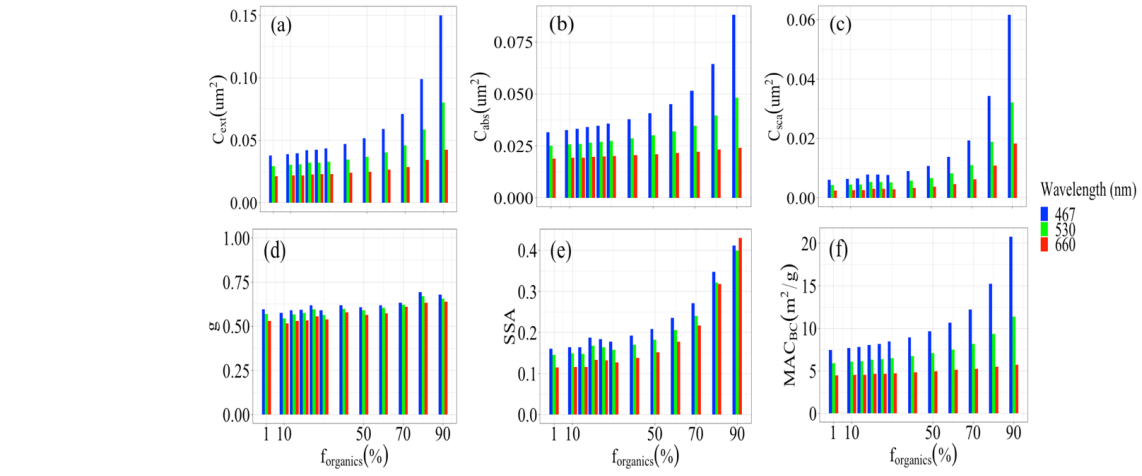

Figure 10. Spectral dependency of coated BCFAs radiative properties (N_s = 200, D_f = 1.7) on fraction of organics ($f_{organics}$): extinction cross-section C_{ext} (a), absorption cross-section C_{abs} (b), scattering cross-section C_{sca} (c), asymmetry parameter g (d), single scattering albedo SSA (e), and black carbon mass absorption cross-section MAC_{BC} (f). For the variability (%) refer to the case D_f = 1.7 in Table 2.

3.6 Ångstrom absorption exponent (AAE) and enhancement factors (E_λ)

Figure 11 shows the Ångstrom absorption exponent (AAE) of a chain-like BCFA (D_f = 1.7) as a function of mobility diameter (D_{mob}), and increasing fraction of organics ($f_{organic}$). The AAE is derived from the slope of C_{abs} vs λ at 467, 530, and 660 nm. As expected, the AAE shows a coherent dependency on the fraction of organics ($f_{organic}$). In this case, the values of AAE vary from 1.4 up to 3.6 with increase in $f_{organic}$ from 1% until 90%. The variability in the modelled values of AAE may be attributed to the selection of the refractive indices and wavelengths (Liu et al., 2018). Similar result for the Ångstrom absorption exponent (AAE) of a more compact BCFA (D_f = 2.2) is provided in the Fig. S6. Additionally, the impact of morphology or fractal dimension (D_f) on the AAE for pure BCFAs is shown in Fig. 12. The values range from 1.06 to 1.47 in this case. It is observed that in smaller BCFA, the AAE increases as the BCFA becomes more compact, whereas in larger BCFA an opposite effect is seen. Fig. 11 and 12 closely represents the ageing process of BC in the atmosphere focusing on changing composition and shape respectively.

Figure 13 shows the trend in absorption enhancement factors (E_λ) as a function of mobility diameter (D_{mob}) and increasing fraction of organics ($f_{organic}$) for a BCFA (D_f = 1.7). The top row shows the absorption enhancement factors calculated from the results of the MSTM code (E^{λ}_{MSTM}) whereas, the ones derived from the Mie calculations (E^{λ}_{Mie}) are displayed in the bottom row. In general, the Mie derived absorption enhancement factors are larger by a factor of 1.1 to 1.5. The enhancement results from both MSTM and Mie calculations are shown for three wavelengths i.e. 660, 530, and 467nm (right to left). There is an expected increase in the absorption enhancement factors as the wavelength decreases. The values of the modelled absorption enhancement factors follow the results from various ambient studies which measured enhancement factors ranging from 1.0 to 2.25 at wavelengths between 532nm to 678nm (Cappa et al., 2012; Cui et al., 2016; Wu et al., 2018).

https://doi.org/10.5194/acp-2020-1290
Preprint. Discussion started: 15 January 2021

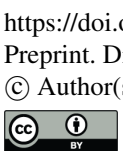

Atmospheric Chemistry and Physics Discussions

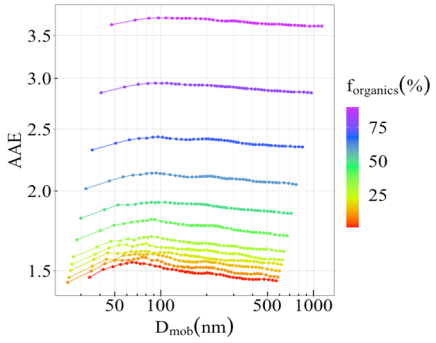

Figure 11. Ångstrom absorption exponent (AAE) of coated BCFAs (D_f= 1.7) with changing fraction of organics ($f_{organics}$) and mobility diameter (D_{mob}).

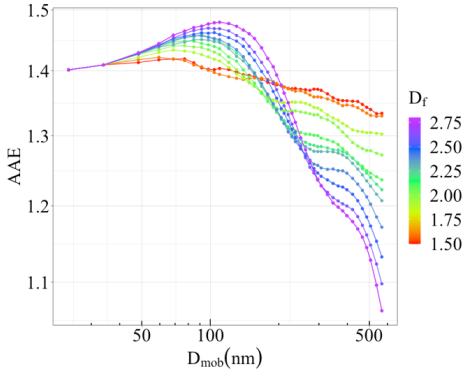

Figure 12. Ångstrom absorption exponent (AAE) of pure BCFAs ($f_{coating}$ = 0%) with changing fractal dimension (D_f) and mobility diameter (D_{mob}).

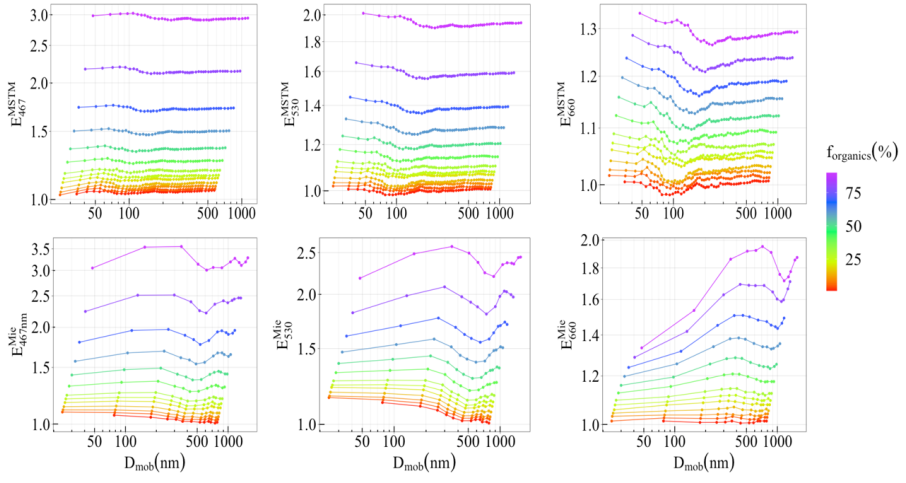

Figure 13. Absorption enhancement factor (E_λ) in BCFAs (D_f= 1.7) with changing fraction of organics ($f_{organics}$) and mobility diameter (D_{mob}). The top row shows the E_λ derived from the MSTM method whereas the ones derived

https://doi.org/10.5194/acp-2020-1290
Preprint. Discussion started: 15 January 2021

Atmospheric Chemistry and Physics Discussions

from Mie code are shown in the bottom row. The enhancement factors are shown for wavelengths equal to 660, 530, and 467nm (right to left).

3.7 Implications over black carbon radiative forcing

In this section, the dependence of the black carbon radiative forcing on modifying composition and morphology of BCFAs is discussed. The relative changes in the top of the atmosphere radiative forcing (ΔF_{TOA}) are quantified as a function of fractal dimension (D_f) and fraction of organics ($f_{organics}$). It is a sensitivity analysis, applicable mostly to scenarios with high urban pollutions. The black carbon radiative forcing at the top of the atmosphere (ΔF_{TOA}) is estimated using equation (14) with fixed values of S_o = 1368 Wm^{-2}, N_{cloud}=0.6, T = 0.79, τ = 0.03, and a = 0.1 (Chylek and Wong, 1995; Lesins et al., 2002). To focus primarily on radiative effects of BC, the optical depth τ is taken as 0.03 for smoke aerosol (Penner et al., 1992). The values of β and ω change with fractal dimension (D_f) and fraction of organics ($f_{organics}$), and are obtained from the MSTM bulk radiative properties. The bulk radiative properties are calculated at a wavelength of 530 nm, over a lognormal polydisperse size distribution with the geometric mean radius (r_o) and standard deviation (σ) fixed to 0.12μm and 1.5, respectively. The details about the bulk radiative properties can be found in the supplementary material of this work.

Table. 3 shows how the values of black carbon radiative forcing change for various morphologies represented by fractal dimension (D_f) for pure black carbon. This can be further understood by the relative change (C) given as:

$$C = \frac{\Delta F_{TOA} - \Delta F_{TOA}^{Ref}}{\Delta F_{TOA}^{Ref}} \times 100 \quad (16)$$

where ΔF_{TOA}^{Ref} is the top of the atmosphere radiative forcing for a reference case where the fractal dimension (D_f) is 1.7 i.e., a freshly emitted black carbon particle.

Table 3. Black carbon radiative forcing ΔF_{TOA} (Wm^{-2}) calculated at various fractal dimension (D_f) and relative change (C) with respect to a reference case with D_f =1.7.

D_f	ΔF_{TOA}	C (%)
1.5	0.704	-1.1
1.6	0.721	-2.3
1.8	0.697	-3.4
1.9	0.681	-5.6
2	0.649	-9.9
2.1	0.608	-15.7
2.2	0.581	-19.4
2.3	0.570	-21.0
2.4	0.507	-29.7
2.5	0.446	-38.2
2.6	0.383	-46.9
2.7	0.324	-55.1
2.8	0.279	-61.2

Similarly, the values of black carbon radiative forcing for various compositions represented by fraction of organics ($f_{organics}$) in a case where the fractal dimension (D_f) is fixed to 2.2 is shown in Table. 4. The values of relative change (C) are calculated using equation (16) with respect to ΔF_{TOA}^{Ref} of a case of zero fraction of organics ($f_{organics}$) i.e., pure black carbon particle.

Global models use the simplified core-shell representation for BC (Bond et al., 2013) which is morphologically close to a coated BCFA of D_f 2.8. In the case of coated BCFA, there is a relative change (C) of 20% when D_f increases from 1.5 to 2.2. Following the results in Table. 4 the relative change (C) in ΔF_{TOA} of coated BCFA is also expected to increase as the D_f approaches 2.8. Therefore, the influence of morphology over the ΔF_{TOA} is clearly overlooked while using the simplified core-shell representation of BC.

Even though the simplified radiative model for absorbing aerosols used, the results of relative change (C) in Table 3 and Table 4 can provide insights about the implications of BC ageing on their radiative forcing estimates.

https://doi.org/10.5194/acp-2020-1290
Preprint. Discussion started: 15 January 2021

Atmospheric Chemistry and Physics Discussions

It is demonstrated that the radiative forcing results are highly sensitive towards modifications in morphology and composition when using the aggregate representation. It must be noted that these results are of high relevance in the BC hotspots regions of Asia, for example, Manilla in Philippines, where the BC emission shared up to 70% of calculated PM_1 (particulate matter with diameter < 1µm) mass emission factors (Madueno et al., 2019).

Table 4. Black carbon radiative forcing ΔF_{TOA} (Wm^{-2}) calculated at various fraction of organics ($f_{organics}$) and relative change (C) with respect to a reference case with $f_{organics}$ = 0%.

$f_{organic}$	ΔF_{TOA}	C (%)
1	0.581	-1.6
5	0.572	-1.5
10	0.572	-2.4
15	0.567	-1.6
20	0.572	-2.4
25	0.567	-1.5
30	0.572	-2.3
40	0.568	-5.1
50	0.552	-10.0
60	0.523	-12.8
70	0.507	-19.0
80	0.471	-32.8
90	0.391	-54.6

3.8 Parametrization scheme for coated BCFAs

In this section, the optimal fits for the results of the radiative properties obtained from the MSTM code are discussed. Since the extinction and absorption cross-section scales linearly with size or D_{mob} in both Fig. 5 and 7, a first order polynomial on log scales was found to be the best fit.

$$lnC_{ext} = c_0 + c_1 lnD_{mob} \quad (17)$$

$$lnC_{abs} = g_0 + g_1 lnD_{mob} \quad (18)$$

For the results of scattering cross-section (C_{sca}) and SSA, a fit of logarithmic D_{mob} with a linear offset was used. The asymmetry parameter (g) is well captured by a cubic polynomial in the logarithm of D_{mob}.

$$lnC_{sca} = H_0 + H_1 lnD_{mob} + H_2 \ln(lnD_{mob}) \quad (19)$$

$$lnSSA = k_0 + k_1 lnD_{mob} + k_2 \ln(lnD_{mob}) \quad (20)$$

$$lng = \sum_{n=0}^{3} s_n lnD_{mob}^n \quad (21)$$

Since the nature of the curve for mass absorption cross-section (MAC_{BC}) changes for various D_f, it was not possible to find an optimal function representative for the entire dataset. For all the other fits, the data is omitted where D_{mob} < 50nm to reduce the resulting root-means-square errors (RMSEs), also suggested by Smith and Grainger, 2014. Previous studies have also attempted to fit the radiative properties of pure BCFAs with respect to the number of primary particles (N_s) (Smith and Grainger, 2014; Kahnert, 2012b). In this study, the parametrization for cross-sections, *SSA*, and g of pure and coated BCFAs with respect to D_{mob} is provided. The above-mentioned fits were applied over the entire dataset, for all the wavelengths (λ), fractal dimensions (D_f) and fraction of organics ($f_{organics}$) used in our classification. The parametrization is presented as a Supplement to this work, providing the user an option to choose among the various cases of λ, D_f and $f_{organics}$.

https://doi.org/10.5194/acp-2020-1290
Preprint. Discussion started: 15 January 2021

Atmospheric Chemistry and Physics Discussions

3.8.1 Error analysis of the parametrization scheme

In this scheme, the parametrization for radiative properties of BCFAs are provided for each point of the classification given in Fig. 1. In the case of pure BCFAs, the parametrization is provided for all combinations of λ (nm)= {467, 530, 660}, and D_f = {1.5, 1.6, 1.7, 1.8, 1.9, 2.2, 2.1, 2.3, 2.4, 2.5, 2.6, 2.7, 2.8}. Whereas, in the coated BCFAs, for all combinations of λ (nm) = {467, 530, 660}; D_f = {1.5, 1.6, 1.7, 1.8, 1.9, 2.2} and $f_{organics}$ (%) = {1, 5, 10, 15, 20, 25, 30, 40, 50, 60, 70, 80, 90}. This scheme is named as P_I and provides the user an advantage to select among various cases, suitable for their purpose.

In order to examine and test the P_I scheme, the relative root mean square errors (RMSEs) between the MSTM modelled and fitted values of radiative properties were measured. Fig. 14 shows the values of relative RMSEs over a range of D_{mob} for the cases of λ (nm) = {660}; $f_{organics}$ (%) = {50}; and D_f = {1.5, 1.6, 1.7, 1.8, 1.9, 2.2}. For the entire range of D_{mob} and D_f, the errors in cross-sections are less than 1%. The relative RMSE is < 2.5% for SSA and up to 16% for g.

Similarly, relative RMSE values for the entire range of $f_{organic}$ can be seen from Fig. 15. In this case, the values of λ (nm)= {660}; D_f = {1.7}; and $f_{organics}$ (%) = {1, 5, 10, 15, 20, 25, 30, 40, 50, 60, 70, 80, 90} were used. The errors in the cross-sections are comparable to Fig. 11, being < 1.5% in all cases. Similarly, the relative RMSE for SSA is < 3%. The error in g peaks to 18% at $f_{organics}$ < 20% for larger sizes.

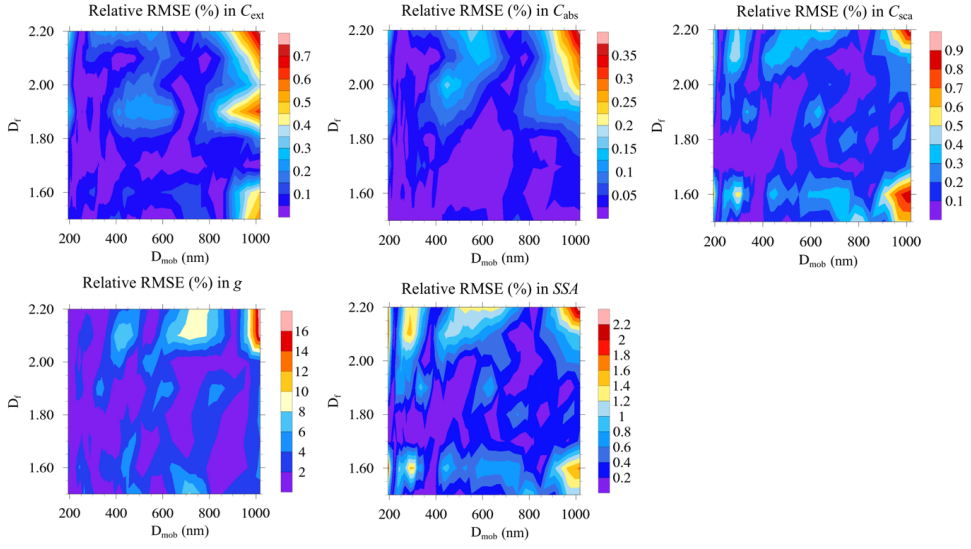

Figure 14. The relative RMSE between MSTM modelled and parametrized values of C_{ext}, C_{abs}, C_{sca}, g, and SSA for various cases of fractal dimension (D_f) at λ = 660nm. The fraction of organics ($f_{organics}$) is fixed to 50%.

https://doi.org/10.5194/acp-2020-1290
Preprint. Discussion started: 15 January 2021

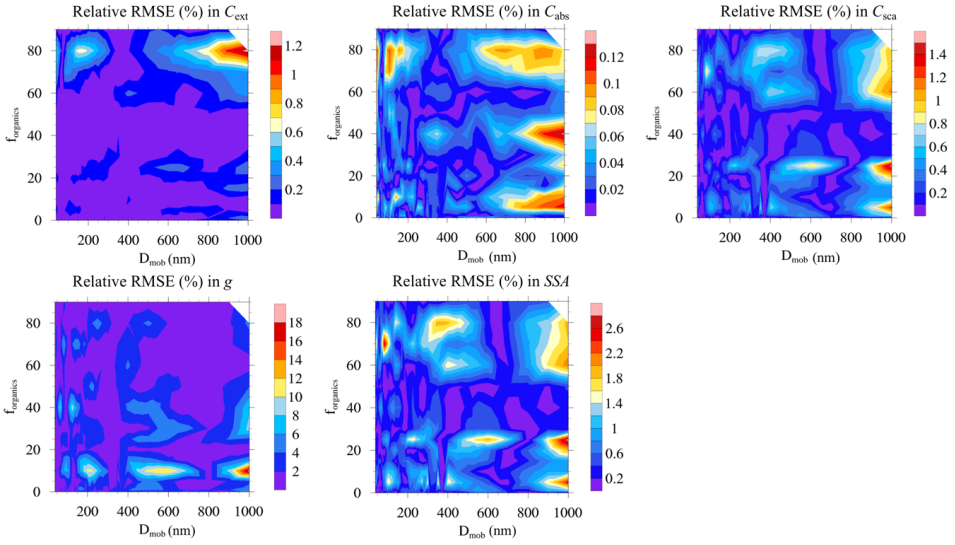

Figure 15. The relative RMSE between MSTM modelled and parametrized values of C_{ext}, C_{abs}, C_{sca}, g, and SSA for various cases of fraction of organics ($f_{organics}$) at λ = 660nm. The fractal dimension (D_f) is fixed to 1.7.

It is better to have a large dataset of BCFA radiative properties with smaller step size in the range of parameters for developing parametrization schemes. To demonstrate this, the P_I scheme is compared to another scheme P_{II}. In the P_{II} scheme, the same fits are applied to the averaged values of radiative properties over a range of D_f and $f_{organics}$ i.e. a lower resolution dataset. The P_{II} scheme was applied over the radiative properties of a group of BCFAs with D_f = 1.5-1.7, and $f_{organics}$ = 60-90% to obtain the "averaged" fit coefficients. The errors from this parametrization scheme P_{II} were compared to the errors from their equivalent inclusive case of a BCFA (D_f = 1.7, and $f_{organics}$ = 60%) in the original parametrization scheme P_I. The results are summarized in the table 2. The relative RMSE errors from the P_{II} are evidently larger than the ones from P_I, validating the requirement for a larger dataset with higher resolution for developing parametrization schemes to minimize errors.

Table 5. Comparison between the Relative RMSE errors of parametrization schemes over a single case of BCFA (D_f = 1.7, $f_{organics}$ = 60%, and λ = 660nm). The errors on the left (P_I) are for the original scheme developed in this study. Whereas the errors on right show the errors resulting from P_{II}, which is the condensed form of P_I i.e. D_f = 1.5-1.7, and $f_{organics}$ = 60-90%. The relative RMSE errors from P_{II} are significantly higher than P_I, emphasizing the need of a larger dataset as the one used in this study, for developing parametrization schemes.

Radiative property	Relative RMSE (%)	
	P_I	P_{II}
C_{ext}	0.09	4.98
C_{abs}	0.02	1.42
C_{sca}	0.30	9.23
g	1.17	8.46
SSA	0.68	7.12

4 Conclusions

Radiative properties of pure and coated BCFAs were systematically investigated as a function of particle size (D_{mob}), primary particle size (a_o), morphology (D_f), composition ($f_{organics}$), and wavelength (λ), further developing a comprehensive parametrization scheme.

In contrary to the BCFA of fixed volume, the modelled radiative properties of BCFAs were found to be sensitive to changes in the radius of the primary particle (a_o) at a fixed D_{mob}. The absorption cross-section C_{abs} increased

https://doi.org/10.5194/acp-2020-1290
Preprint. Discussion started: 15 January 2021

Atmospheric Chemistry and Physics Discussions

by a factor of almost ten from a_o equal to 15nm to 30nm. Amongst size (or D_{mob}), morphology (or D_f), and composition (or $f_{organics}$), the dependency on size was found dominant in all the radiative properties of BCFAs. This is evident from the increase in cross-sections from 0.0001μm^2 to 0.1μm^2 for BCFA D_{mob} ranging from 24nm to 810nm. In terms of morphology, the C_{sca}, SSA, and g showed the highest sensitivity towards D_f, pronouncing as the BCFA grows in size. The factor of changing morphology is overlooked when using the Mie theory for calculation of BC radiative properties in global models. The SSA showed values of up to 0.42. In contrary, the C_{ext}, C_{abs}, and MAC_{BC} were more sensitive with respect to changing composition of BCFAs. The values of MAC_{BC} increased by a factor of 1.5 with increasing amount of $f_{organics}$ up to 90%, at λ = 660nm.

In the visible range, all the radiative properties decreased with λ. However, the behavior of spectral dependency with respect to the changing morphology and composition varied. The asymmetry parameter (g) showed the highest sensitivity of spectral dependence on morphology or D_f, dominant at a higher D_f, i.e. for compact aggregates. The increase of g (from λ = 467nm to 660nm) changes from a factor of 1.1 to 2.6 for lower to higher values of D_f respectively. Whereas, all the cross-sections and black carbon mass absorption cross-section MAC_{BC} showed a significant increase in the spectral dependency with composition or $f_{organics}$. This spectral dependency of $f_{organics}$ can increase the cross-sections up to a factor of 4. MAC_{BC} showed values of up to 20 m^2/g for the extreme case of 90% $f_{organics}$ at λ = 467nm. Additionally, at lower wavelengths (467nm), the MAC_{BC} may increase up to a factor of 2.6 with increase in $f_{organics}$.

The values of AAE changed from 1.06 up to 3.6 depending on the fraction of organics ($f_{organic}$), fractal dimension (D_f), and size (D_{mob}). The Mie calculation derived absorption enhancement factors (E_λ) were larger by a factor of 1.1 to1.5 to their equivalent MSTM method derived values. The values of the absorption enhancement factor (E_λ) varied from 1.0 to 3.28 as a function of wavelength (λ) and size (D_{mob}).

The implications of modifying the composition and morphology of BCFAs over the black carbon radiative forcing were discussed. The black carbon radiative forcing ΔF_{TOA} (Wm^{-2}) can decrease up to 61% as the BCFA becomes more compact in morphology i.e., a higher fractal dimension (D_f). Therefore, the influence of morphology over the top of the atmosphere radiative forcing is overlooked while using the simplified core-shell representation of BC. Whereas, there is a decrease > 50% in ΔF_{TOA} as the organic content of particle decreases i.e., a higher fraction of organics ($f_{organic}$). The findings are particularly relevant for modellers of urban pollution.

It is observed that the impact of BC particle becoming more compact, and increase in organic content go in the same direction i.e., decrease in the ΔF_{TOA}. This could cause changes in the dynamics of boundary layer in some scenarios. Therefore, these factors must be kept under consideration while designing the BC simulation and further discussing the radiative impacts using global models.

The novel parametrization scheme developed in this work can be used for modelling, ambient, and laboratory-based radiative studies of BC. The parametrization scheme provides a high resolution, giving the user a wider parameter space to select from. The parametrised radiative properties showed a low relative RMSEs with respect to the original MSTM derived values. For the entire parametrization scheme, the RMSEs in cross-sections were less than 1%. Similarly, the relative RMSE for SSA was < 3%. The error in g peaks to 18% at $f_{organics}$ < 20% for larger sizes. However, it is acknowledged that the results from the parametrization scheme might vary to the results from laboratory and ambient measurements. To understand the nature of discrepancy in modelled radiative properties, it is suggested that they must be compared and validated to their equivalent laboratory or ambient results. This can be done by conducting parallel modelling and laboratory-based investigation of BCFAs, focussing on the various factors (size, morphology, and composition) that influence the radiative properties as discussed in this study.

Acknowledgement

This work is supported by the 16ENV02 Black Carbon project of the European Union through the European Metrology Programme for Innovation and Research (EMPIR).

References

Abel, S. J., Haywood, J. M., Highwood, E. J., Li, J. and Buseck, P. R.: Evolution of biomass burning aerosol properties from an agricultural fire in southern Africa, Geophys. Res. Lett., doi:10.1029/2003GL017342, 2003.

Adachi, K., Chung, S. H. and Buseck, P. R.: Shapes of soot aerosol particles and implications for their effects on climate, J. Geophys. Res. Atmos., doi:10.1029/2009JD012868, 2010.

https://doi.org/10.5194/acp-2020-1290
Preprint. Discussion started: 15 January 2021

Atmospheric Chemistry and Physics Discussions

720 Alexander, D. T. L., Crozier, P. A. and Anderson, J. R.: Brown carbon spheres in East Asian outflow and their
721 radiative properties, Science (80-.)., doi:10.1126/science.1155296, 2008.

722 Appel, B. R., Tokiwa, Y., Hsu, J., Kothny, E. L. and Hahn, E.: Visibility as related to atmospheric aerosol
723 constituents, Atmos. Environ., doi:10.1016/0004-6981(85)90290-2, 1985.

724 Bambha, R. P., Dansson, M. A., Schrader, P. E. and Michelsen, H. A.: Effects of volatile coatings on the laser-
725 induced incandescence of soot, Appl. Phys. B Lasers Opt., doi:10.1007/s00340-013-5463-9, 2013.

726 Bescond, A., Yon, J., Ouf, F. X., Ferry, D., Delhaye, D., Gaffié, D., Coppalle, A. and Rozé, C.: Automated
727 determination of aggregate primary particle size distribution by tem image analysis: Application to soot,
728 Aerosol Sci. Technol., doi:10.1080/02786826.2014.932896, 2014.

729 Bockhorn, H.: Combustion generated fine carbonaceous particles, KIT Scientific Publishing, Karlsruhe., 2009.

730 Bond, T. C. and Bergstrom, R. W.: Light absorption by carbonaceous particles: An investigative review, Aerosol
731 Sci. Technol., doi:10.1080/02786820500421521, 2006.

732 Bond, T. C., Bhardwaj, E., Dong, R., Jogani, R., Jung, S., Roden, C., Streets, D. G. and Trautmann, N. M.:
733 Historical emissions of black and organic carbon aerosol from energy-related combustion, 1850-2000,
734 Global Biogeochem. Cycles, doi:10.1029/2006GB002840, 2007.

735 Bond, T. C., Doherty, S. J., Fahey, D. W., Forster, P. M., Berntsen, T., Deangelo, B. J., Flanner, M. G., Ghan, S.,
736 Kärcher, B., Koch, D., Kinne, S., Kondo, Y., Quinn, P. K., Sarofim, M. C., Schultz, M. G., Schulz, M.,
737 Venkataraman, C., Zhang, H., Zhang, S., Bellouin, N., Guttikunda, S. K., Hopke, P. K., Jacobson, M. Z.,
738 Kaiser, J. W., Klimont, Z., Lohmann, U., Schwarz, J. P., Shindell, D., Storelvmo, T., Warren, S. G. and
739 Zender, C. S.: Bounding the role of black carbon in the climate system: A scientific assessment, J. Geophys.
740 Res. Atmos., doi:10.1002/jgrd.50171, 2013.

741 Calcote, H. F.: Mechanisms of soot nucleation in flames-A critical review, Combust. Flame, doi:10.1016/0010-
742 2180(81)90159-0, 1981.

743 Cappa, C. D., Onasch, T. B., Massoli, P., Worsnop, D. R., Bates, T. S., Cross, E. S., Davidovits, P., Hakala, J.,
744 Hayden, K. L., Jobson, B. T., Kolesar, K. R., Lack, D. A., Lerner, B. M., Li, S. M., Mellon, D., Nuaaman,
745 I., Olfert, J. S., Petäjä, T., Quinn, P. K., Song, C., Subramanian, R., Williams, E. J. and Zaveri, R. A.:
746 Radiative absorption enhancements due to the mixing state of atmospheric black carbon, Science (80-.).,
747 doi:10.1126/science.1223447, 2012.

748 Chakrabarty, R. K., Moosmüller, H., Garro, M. A., Arnott, W. P., Walker, J., Susott, R. A., Babbitt, R. E., Wold,
749 C. E., Lincoln, E. N. and Hao, W. M.: Emissions from the laboratory combustion of wildland fuels: Particle
750 morphology and size, J. Geophys. Res. Atmos., doi:10.1029/2005JD006659, 2006.

751 China, S., Mazzoleni, C., Gorkowski, K., Aiken, A. C. and Dubey, M. K.: Morphology and mixing state of
752 individual freshly emitted wildfire carbonaceous particles, Nat. Commun., doi:10.1038/ncomms3122, 2013.

753 Chylek, P. and Wong, J.: Effect of absorbing aerosols on global radiation budget, Geophys. Res. Lett.,
754 doi:10.1029/95GL00800, 1995.

755 Cui, X., Wang, X., Yang, L., Chen, B., Chen, J., Andersson, A. and Gustafsson, Ö.: Radiative absorption
756 enhancement from coatings on black carbon aerosols, Sci. Total Environ.,
757 doi:10.1016/j.scitotenv.2016.02.026, 2016.

758 Doherty, S. J., Warren, S. G., Grenfell, T. C., Clarke, A. D. and Brandt, R. E.: Light-absorbing impurities in Arctic
759 snow, Atmos. Chem. Phys., doi:10.5194/acp-10-11647-2010, 2010.

https://doi.org/10.5194/acp-2020-1290
Preprint. Discussion started: 15 January 2021

Atmospheric Chemistry and Physics Discussions

760 Dong, Z., Kang, S., Qin, D., Shao, Y., Ulbrich, S. and Qin, X.: Variability in individual particle structure and
761 mixing states between the glacier-snowpack and atmosphere in the northeastern Tibetan Plateau,
762 Cryosphere, doi:10.5194/tc-12-3877-2018, 2018.

763 Düsing, S., Wehner, B., Seifert, P., Ansmann, A., Baars, H., Ditas, F., Henning, S., Ma, N., Poulain, L., Siebert,
764 H., Wiedensohler, A. and MacKe, A.: Helicopter-borne observations of the continental background aerosol
765 in combination with remote sensing and ground-based measurements, Atmos. Chem. Phys.,
766 doi:10.5194/acp-18-1263-2018, 2018.

767 Fierce, L., Riemer, N. and Bond, T. C.: Explaining variance in black carbon's aging timescale, Atmos. Chem.
768 Phys., doi:10.5194/acp-15-3173-2015, 2015.

769 Forrest, S. R. and Witten, T. A.: Long-range correlations in smoke-particle aggregates, J. Phys. A Gen. Phys.,
770 doi:10.1088/0305-4470/12/5/008, 1979.

771 Gentner, D. R., Jathar, S. H., Gordon, T. D., Bahreini, R., Day, D. A., El Haddad, I., Hayes, P. L., Pieber, S. M.,
772 Platt, S. M., de Gouw, J., Goldstein, A. H., Harley, R. A., Jimenez, J. L., Prévôt, A. S. H. and Robinson, A.
773 L.: Review of Urban Secondary Organic Aerosol Formation from Gasoline and Diesel Motor Vehicle
774 Emissions, Environ. Sci. Technol., 51(3), 1074–1093, doi:10.1021/acs.est.6b04509, 2017.

775 Guarieiro, A. L. N., Eiguren-Fernandez, A., Da Rocha, G. O. and De Andrade, J. B.: An investigation on
776 morphology and fractal dimension of diesel and diesel-biodiesel soot agglomerates, J. Braz. Chem. Soc.,
777 doi:10.21577/0103-5053.20160306, 2017.

778 Gustafson, B. Å. S. and Kolokolova, L.: A systematic study of light scattering by aggregate particles using the
779 microwave analog technique: Angular and wavelength dependence of intensity and polarization, J.
780 Geophys. Res. Atmos., doi:10.1029/1999JD900327, 1999.

781 He, C., Liou, K. N., Takano, Y., Zhang, R., Levy Zamora, M., Yang, P., Li, Q. and Leung, L. R.: Variation of the
782 radiative properties during black carbon aging: Theoretical and experimental intercomparison, Atmos.
783 Chem. Phys., doi:10.5194/acp-15-11967-2015, 2015.

784 Hentschel, H. G. E.: Fractal dimension of generalized diffusion-limited aggregates, Phys. Rev. Lett.,
785 doi:10.1103/PhysRevLett.52.212, 1984.

786 Hess, W. M., Ban, L. L. and McDonald, G. C.: Carbon Black Morphology: I. Particle Microstructure. II.
787 Automated EM Analysis of Aggregate Size and Shape, Rubber Chem. Technol., doi:10.5254/1.3539291,
788 1969.

789 Homann, K. H.: Carbon formation in premixed flames, Combust. Flame, doi:10.1016/0010-2180(67)90017-X,
790 1967.

791 Janssen, N. A. H., Hoek, G., Simic-Lawson, M., Fischer, P., van Bree, L., Brink, H. Ten, Keuken, M., Atkinson,
792 R. W., Ross Anderson, H., Brunekreef, B. and Cassee, F. R.: Black carbon as an additional indicator of the
793 adverse health effects of airborne particles compared with pm10 and pm2.5, Environ. Health Perspect.,
794 doi:10.1289/ehp.1003369, 2011.

795 Kahnert, M.: Numerically exact computation of the radiative properties of light absorbing carbon aggregates for
796 wavelength of 200 nm-12.2 μm, Atmos. Chem. Phys., doi:10.5194/acp-10-8319-2010, 2010.

797 Kahnert, M.: On the discrepancy between modeled and measured mass absorption cross sections of light absorbing
798 carbon aerosols, Aerosol Sci. Technol., doi:10.1080/02786821003733834, 2010.

799 Kim, J., Bauer, H., Dobovičnik, T., Hitzenberger, R., Lottin, D., Ferry, D. and Petzold, A.: Assessing radiative
800 properties and refractive index of combustion aerosol particles through combined experimental and
801 modeling studies, Aerosol Sci. Technol., doi:10.1080/02786826.2015.1020996, 2015.

https://doi.org/10.5194/acp-2020-1290
Preprint. Discussion started: 15 January 2021

Atmospheric Chemistry and Physics Discussions

802 Klimont, Z., Kupiainen, K., Heyes, C., Purohit, P., Cofala, J., Rafaj, P., Borken-Kleefeld, J. and Schöpp, W.:
803 Global anthropogenic emissions of particulate matter including black carbon, Atmos. Chem. Phys.,
804 doi:10.5194/acp-17-8681-2017, 2017.

805 Kumar, M., Parmar, K. S., Kumar, D. B., Mhawish, A., Broday, D. M., Mall, R. K. and Banerjee, T.: Long-term
806 aerosol climatology over Indo-Gangetic Plain: Trend, prediction and potential source fields, Atmos.
807 Environ., doi:10.1016/j.atmosenv.2018.02.027, 2018.

808 Lesins, G., Chylek, P. and Lohmann, U.: A study of internal and external mixing scenarios and its effect on aerosol
809 optical properties and direct radiative forcing, J. Geophys. Res. Atmos., doi:10.1029/2001jd000973, 2002.

810 Li, J., Liu, C., Yin, Y. and Kumar, K. R.: Numerical investigation on the Ångström exponent of black carbon
811 aerosol, J. Geophys. Res., doi:10.1002/2015JD024718, 2016.

812 Liati, A., Brem, B. T., Durdina, L., Vögtli, M., Dasilva, Y. A. R., Eggenschwiler, P. D. and Wang, J.: Electron
813 microscopic study of soot particulate matter emissions from aircraft turbine engines, Environ. Sci. Technol.,
814 doi:10.1021/es501809b, 2014.

815 Liu, C., Chung, C. E., Yin, Y. and Schnaiter, M.: The absorption Ångström exponent of black carbon: From
816 numerical aspects, Atmos. Chem. Phys., doi:10.5194/acp-18-6259-2018, 2018.

817 Liu, C., Panetta, R. L. and Yang, P.: The influence of water coating on the radiative scattering properties of fractal
818 soot aggregates, Aerosol Sci. Technol., doi:10.1080/02786826.2011.605401, 2012.

819 Liu, C., Yin, Y., Hu, F., Jin, H. and Sorensen, C. M.: The Effects of Monomer Size Distribution on the Radiative
820 Properties of Black Carbon Aggregates, Aerosol Sci. Technol., doi:10.1080/02786826.2015.1085953,
821 2015.

822 Liu, L. and Mishchenko, M. I.: Scattering and radiative properties of morphologically complex carbonaceous
823 aerosols: A systematic modeling study, Remote Sens., doi:10.3390/rs10101634, 2018.

824 Luo, J., Zhang, Y., Wang, F., Wang, J. and Zhang, Q.: Applying machine learning to estimate the radiative
825 properties of black carbon fractal aggregates, J. Quant. Spectrosc. Radiat. Transf.,
826 doi:10.1016/j.jqsrt.2018.05.002, 2018.

827 Luo, J., Zhang, Y., Zhang, Q., Wang, F., Liu, J. and Wang, J.: Sensitivity analysis of morphology on radiative
828 properties of soot aerosols, Opt. Express, doi:10.1364/oe.26.00a420, 2018.

829 Ma, N., Zhao, C. S., Nowak, A., Müller, T., Pfeifer, S., Cheng, Y. F., Deng, Z. Z., Liu, P. F., Xu, W. Y., Ran, L.,
830 Yan, P., Göbel, T., Hallbauer, E., Mildenberger, K., Henning, S., Yu, J., Chen, L. L., Zhou, X. J., Stratmann,
831 F. and Wiedensohler, A.: Aerosol radiative properties in the North China Plain during HaChi campaign: An
832 in-situ radiative closure study, Atmos. Chem. Phys., doi:10.5194/acp-11-5959-2011, 2011.

833 Mackowski, D. W. and Mishchenko, M. I.: A multiple sphere T-matrix Fortran code for use on parallel computer
834 clusters, J. Quant. Spectrosc. Radiat. Transf., doi:10.1016/j.jqsrt.2011.02.019, 2011.

835 Mackowski, D. W.: MSTM Version 3.0: April 2013, available at:
836 http://www.eng.auburn.edu/~dmckwski/scatcodes/ (last access: 10 October 2017), 2013.

837 Madueño, L., Kecorius, S., Birmili, W., Müller, T., Simpas, J., Vallar, E., Galvez, M. C., Cayetano, M. and
838 Wiedensohler, A.: Aerosol particle and black carbon emission factors of vehicular fleet in Manila,
839 Philippines, Atmosphere (Basel)., doi:10.3390/atmos10100603, 2019.

840 Madueño, L., Kecorius, S., Birmili, W., Müller, T., Simpas, J., Vallar, E., Galvez, M. C., Cayetano, M. and
841 Wiedensohler, A.: Aerosol particle and black carbon emission factors of vehicular fleet in Manila,
842 Philippines, Atmosphere (Basel)., doi:10.3390/atmos10100603, 2019.

https://doi.org/10.5194/acp-2020-1290
Preprint. Discussion started: 15 January 2021

Atmospheric Chemistry and Physics Discussions

Mariusz Woźniak. Characterization of nanoparticle aggregates with light scattering techniques. Optics [physics.optics]. Aix-Marseille Université, 2012. English. fftel00747711f.

Mie, G.: On the optics of turbid media, especially colloidal metal solutions, Ann. Phys. Berlin, 1908.

Mishchenko, M. I., Liu, L., Travis, L. D. and Lacis, A. A.: Scattering and radiative properties of semi-external versus external mixtures of different aerosol types, J. Quant. Spectrosc. Radiat. Transf., doi:10.1016/j.jqsrt.2003.12.032, 2004.

Mishchenko, M. I., Travis, L. D. and Lacis, A. a: Scattering, Absorption, and Emission of Light by Small Particles, Vasa, 2002.

Moosmüller, H., Chakrabarty, R. K. and Arnott, W. P.: Aerosol light absorption and its measurement: A review, J. Quant. Spectrosc. Radiat. Transf., doi:10.1016/j.jqsrt.2009.02.035, 2009.

Ouf, F. X., Parent, P., Laffon, C., Marhaba, I., Ferry, D., Marcillaud, B., Antonsson, E., Benkoula, S., Liu, X. J., Nicolas, C., Robert, E., Patanen, M., Barreda, F. A., Sublemontier, O., Coppalle, A., Yon, J., Miserque, F., Mostefaoui, T., Regier, T. Z., Mitchell, J. B. A. and Miron, C.: First in-flight synchrotron X-ray absorption and photoemission study of carbon soot nanoparticles, Sci. Rep., doi:10.1038/srep36495, 2016.

Peng, J., Hu, M., Guo, S., Du, Z., Shang, D., Zheng, J., Zheng, J., Zeng, L., Shao, M., Wu, Y., Collins, D. and Zhang, R.: Ageing and hygroscopicity variation of black carbon particles in Beijing measured by a quasi-atmospheric aerosol evolution study (QUALITY) chamber, Atmos. Chem. Phys., doi:10.5194/acp-17-10333-2017, 2017.

Penner, J. E., Dickinson, R. E. and O'Neill, C. A.: Effects of aerosol from biomass burning on the global radiation budget, Science (80-.)., doi:10.1126/science.256.5062.1432, 1992.

Petzold, A., Gysel, M., Vancassel, X., Hitzenberger, R., Puxbaum, H., Vrochticky, S., Weingartner, E., Baltensperger, U. and Mirabel, P.: On the effects of organic matter and sulphur-containing compounds on the CCN activation of combustion particles, Atmos. Chem. Phys., doi:10.5194/acp-5-3187-2005, 2005.

Ramanathan, V. and Carmichael, G.: Global and regional climate changes due to black carbon, Nat. Geosci., doi:10.1038/ngeo156, 2008.

Rudich, Y., Donahue, N. M. and Mentel, T. F.: Aging of organic aerosol: Bridging the gap between laboratory and field studies, Annu. Rev. Phys. Chem., doi:10.1146/annurev.physchem.58.032806.104432, 2007.

Safai, P. D., Devara, P. C. S., Raju, M. P., Vijayakumar, K. and Rao, P. S. P.: Relationship between black carbon and associated radiative, physical and radiative properties of aerosols over two contrasting environments, Atmos. Res., doi:10.1016/j.atmosres.2014.07.006, 2014.

Sagan, C. and Pollack, J. B.: Anisotropic nonconservative scattering and the clouds of Venus, J. Geophys. Res., doi:10.1029/jz072i002p00469, 1967.

Saleh, R., Marks, M., Heo, J., Adams, P. J., Donahue, N. M. and Robinson, A. L.: Contribution of brown carbon and lensing to the direct radiative effect of carbonaceous aerosols from biomass and biofuel burning emissions, J. Geophys. Res., doi:10.1002/2015JD023697, 2015.Scarnato, B. V., Vahidinia, S., Richard, D. T. and Kirchstetter, T. W.: Effects of internal mixing and aggregate morphology on radiative properties of black carbon using a discrete dipole approximation model, Atmos. Chem. Phys., doi:10.5194/acp-13-5089-2013, 2013.

Shiraiwa, M., Kondo, Y., Iwamoto, T. and Kita, K.: Amplification of light absorption of black carbon by organic coating, Aerosol Sci. Technol., doi:10.1080/02786820903357686, 2010.

Siegmann, K., Sattler, K. and Siegmann, H. C.: Clustering at high temperatures: Carbon formation in combustion, J. Electron Spectros. Relat. Phenomena, doi:10.1016/S0368-2048(02)00152-4, 2002.

https://doi.org/10.5194/acp-2020-1290
Preprint. Discussion started: 15 January 2021

Smith, A. J. A. and Grainger, R. G.: Simplifying the calculation of light scattering properties for black carbon fractal aggregates, Atmos. Chem. Phys., doi:10.5194/acp-14-7825-2014, 2014.

Sorensen, C. M.: Light scattering by fractal aggregates: A review, Aerosol Sci. Technol., doi:10.1080/02786820117868, 2001.

Stier, P., Feichter, J., Kinne, S., Kloster, S., Vignati, E., Wilson, J., Ganzeveld, L., Tegen, I., Werner, M., Balkanski, Y., Schulz, M. and Boucher, O.: The aerosol-climate model ECHAM5-HAM, Atmos. Chem. Phys. Discuss., doi:10.5194/acpd-4-5551-2004, 2004.

Thouy, R. and Jullien, R.: A cluster-cluster aggregation model with tunable fractal dimension, J. Phys. A. Math. Gen., doi:10.1088/0305-4470/27/9/012, 1994.

Wang, Y., Chen, Y., Wu, Z., Shang, D., Bian, Y., Du, Z., H. Schmitt, S., Su, R., I. Gkatzelis, G., Schlag, P., Hohaus, T., Voliotis, A., Lu, K., Zeng, L., Zhao, C., Rami Alfarra, M., McFiggans, G., Wiedensohler, A., Kiendler-Scharr, A., Zhang, Y. and Hu, M.: Mutual promotion between aerosol particle liquid water and particulate nitrate enhancement leads to severe nitrate-dominated particulate matter pollution and low visibility, Atmos. Chem. Phys., doi:10.5194/acp-20-2161-2020, 2020.

Wang, Y., Liu, F., He, C., Bi, L., Cheng, T., Wang, Z., Zhang, H., Zhang, X., Shi, Z. and Li, W.: Fractal Dimensions and Mixing Structures of Soot Particles during Atmospheric Processing, Environ. Sci. Technol. Lett., doi:10.1021/acs.estlett.7b00418, 2017.

Wentzel, M., Gorzawski, H., Naumann, K. H., Saathoff, H. and Weinbruch, S.: Transmission electron microscopical and aerosol dynamical characterization of soot aerosols, J. Aerosol Sci., doi:10.1016/S0021-8502(03)00360-4, 2003.

Wiedensohler, A., Andrade, M., Weinhold, K., Müller, T., Birmili, W., Velarde, F., Moreno, I., Forno, R., Sanchez, M. F., Laj, P., Ginot, P., Whiteman, D. N., Krejci, R., Sellegri, K. and Reichler, T.: Black carbon emission and transport mechanisms to the free troposphere at the La Paz/El Alto (Bolivia) metropolitan area based on the Day of Census (2012), Atmos. Environ., 194, 158–169, doi:https://doi.org/10.1016/j.atmosenv.2018.09.032, 2018.

Witten, T. A. and Sander, L. M.: Diffusion-limited aggregation, Phys. Rev. B, doi:10.1103/PhysRevB.27.5686, 1983.

Wozniak, M., Onofri, F. R. A., Barbosa, S., Yon, J. and Mroczka, J.: Comparison of methods to derive morphological parameters of multi-fractal samples of particle aggregates from TEM images, J. Aerosol Sci., doi:10.1016/j.jaerosci.2011.12.008, 2012.

Wu, Y., Cheng, T., Liu, D., Allan, J. D., Zheng, L. and Chen, H.: Light Absorption Enhancement of Black Carbon Aerosol Constrained by Particle Morphology, Environ. Sci. Technol., doi:10.1021/acs.est.8b00636, 2018.

Wu, Y., Cheng, T., Zheng, L. and Chen, H.: Models for the radiative simulations of fractal aggregated soot particles thinly coated with non-absorbing aerosols, J. Quant. Spectrosc. Radiat. Transf., doi:10.1016/j.jqsrt.2016.05.011, 2016.

Zanatta, M., Gysel, M., Bukowiecki, N., Müller, T., Weingartner, E., Areskoug, H., Fiebig, M., Yttri, K. E., Mihalopoulos, N., Kouvarakis, G., Beddows, D., Harrison, R. M., Cavalli, F., Putaud, J. P., Spindler, G., Wiedensohler, A., Alastuey, A., Pandolfi, M., Sellegri, K., Swietlicki, E., Jaffrezo, J. L., Baltensperger, U. and Laj, P.: A European aerosol phenomenology-5: Climatology of black carbon radiative properties at 9 regional background sites across Europe, Atmos. Environ., doi:10.1016/j.atmosenv.2016.09.035, 2016.

Zhang, Y., Zhang, Q., Cheng, Y., Su, H., Li, H., Li, M., Zhang, X., Ding, A. and He, K.: Amplification of light absorption of black carbon associated with air pollution, Atmos. Chem. Phys., doi:10.5194/acp-18-9879-2018.